Draft version November 11, 2025
Typeset using LaTeX **twocolumn** style in AASTeX631

Kerr Black Hole Shadows in Dispersive Plasma: Frequency-Dependent Geodesics and Shadow Distortions

Sai Karan M[1] and Sandeep Kumar Kataria[2]

[1] *Indian Institute of Science Education and Research, Pune, India*
[2] *Department of Space, Planetary & Astronomical Sciences and Engineering, Indian Institute of Technology Kanpur, Kanpur 208016, India*

ABSTRACT

The black hole shadow, a direct probe of the event horizon's gravitational influence, has been observationally confirmed by the Event Horizon Telescope (EHT). While theoretical models of shadows in vacuum are mature, real astrophysical black holes like M87* and Sgr A* are enveloped in plasma, which can alter photon trajectories through dispersion. Current understanding, based on foundational work, indicates that only specific plasma distributions allow for an analytical treatment via the separation of the Hamilton-Jacobi equation. In this work, we build upon this framework to systematically investigate the propagation of light rays in Kerr spacetime surrounded by a pressureless, non-magnetized cold plasma. We explicitly derive the separability condition, identifying the exact class of plasma densities that permit a generalized Carter constant. For these models, we compute the photon regions and shadow boundaries, characterizing how the shadow's size and shape deviate from the vacuum case in a frequency-dependent manner. Our results provide analytical benchmarks for the distortion of shadows in dispersive media and determine the critical plasma frequency beyond which the shadow is erased, offering a direct link between observable shadow features and the properties of the ambient plasma environment and providing a foundation for studying more dynamic, non-separable plasma distributions.

Keywords: black holes — plasma physics — shadows — Hamilton-Jacobi — Kerr spacetime

1. INTRODUCTION

Black holes are one of the most spectacular predictions of General Relativity (GR). Since Einstein's formulation of GR in 1915, it has become clear that the curvature of spacetime caused by massive bodies leads to a wide range of fascinating phenomena, from gravitational waves to the existence of event horizons around extremely compact objects. The earliest exact solution of Einstein's field equations was found by Schwarzschild in 1916, describing a static, spherically symmetric black hole (Schwarzschild 1916). This solution provided the first concrete evidence within GR that spacetime could admit regions from which not even light can escape.

Over time, more general black hole spacetimes were discovered. The Reissner–Nordström solution includes charge, while the Kerr solution, discovered by Kerr (1963), describes a rotating black hole. The Kerr metric is of particular astrophysical significance, as most black holes are expected to rotate due to the angular momentum they acquire during their formation or accretion processes.

One of the most striking observable features of black holes is their shadow: the dark region seen against a bright background, formed by the capture of photons whose trajectories cross the event horizon, while others are strongly lensed around it (Bardeen 1973). The propagation of timelike and lightlike geodesics in Kerr spacetime was studied in detail by Carter (1968) using the Hamilton–Jacobi method, which also underpins the derivation of Kerr black hole shadows.

In recent years, these predictions have been tested through direct astronomical observations. The Event Horizon Telescope (EHT) collaboration achieved a breakthrough by imaging the shadows of the supermassive black holes M87* (Event Horizon Telescope Collaboration 2019) and Sgr A* (Event Horizon Telescope

1.sai.karanmukthapuram@students.iiserpune.ac.in
2. skkataria.iit@gmail.com

Collaboration 2022). These observations opened a new era in black hole physics, enabling direct comparison between GR-based shadow models and actual astrophysical data.

These groundbreaking observations highlight the importance of comparing theoretical shadow models with actual data. Long before the EHT, however, the foundations of black hole shadow theory were laid by Synge (1966) and Luminet (1979) for Schwarzschild black hole shadows, and thereafter Bardeen (1973) studied the shadows of Kerr black holes over a bright background, which turned out to deviate from a perfect circle. The past decade has seen an increased focus on analytical investigations, observational studies, and numerical simulations of shadows. For instance, Hioki & Maeda (2009) and Johannsen & Psaltis (2010) explored spin estimation and tests of the no-hair theorem, while Amarilla & Eiroa (2010); Amarilla et al. (2010) and Tsukamoto et al. (2014) analyzed shadows in various modified gravity theories. Propagation effects and photon region structures in Kerr spacetimes surrounded by plasma were studied by Perlick & Tsupko (2015, 2017), and further developed in works such as Cunha & Herdeiro (2018); Cunha et al. (2017a,b) and Abdujabbarov et al. (2016). On the numerical and observational front, Mizuno (2018) demonstrated the potential of shadow imaging to test general relativity, and Johannsen (2016) connected shadow properties of Sgr A* to no-hair theorem tests.

An astrophysical black hole is usually surrounded by a complicated environment (such as a corona, a plasma, and jets), and photons near the black hole have to pass through this before reaching an observer far away. Generally, the influence of these surroundings on astronomical observations cannot be overstated.

In this work, we focus on the deviation of lightlike geodesics in Kerr spacetime in the presence of a non-magnetized, pressureless cold plasma. The plasma modifies photon propagation through an effective refractive index, and under certain conditions still preserves separability of the Hamilton–Jacobi equation, ensuring the existence of a generalized Carter constant. We derive the necessary conditions for such separability, determine the photon region in Boyer–Lindquist coordinates, and discuss the shadow boundary in terms of Bardeen coordinates.

The paper is organized as follows, In Section 2 we describe the Hamiltonian formalism for photon motion and derive the absolutely necessary condition for the propagation of light in a plasma medium(Eq. 7). In Section 3 we obtain the expression for the Carter constant and in this process, determine the form of the distribution of the plasma medium for the separability of the Hamilton Jacobi equation. In Section 4, we obtain the expressions for the shadow orbits described by the impact parameters which help us to confine the photon region. In Section 5 we explicitly plot the shadows for certain plasma models and determine the critical frequency above which no light propagates through the plasma distribution. We conclude with a summary of the paper in Section 6.

We use the summation convention for Greek indices, which take the values $0, 1, 2, 3$. Our choice of signature is $(-,+,+,+)$. We raise and lower Greek indices with the spacetime metric. G is the gravitational constant and c is the vacuum speed of light. We use units such that $\hbar = 1$; i.e., energies have the same unit as frequencies and momentum vectors have the same unit as wave vectors.

2. HAMILTONIAN EQUATION OF LIGHT RAYS IN KERR SPACETIME

2.1. *Condition on plasma distribution for the propagation of light*

Light propagation in a non-magnetized pressureless cold plasma is given by the Hamiltonian,

$$H(x,p) = \frac{1}{2}\left(g^{\mu\nu}(x)p_\mu p_\nu + \omega_p(x)^2\right) \tag{1}$$

Here $g^{\mu\nu}$ are the contravariant components of the spacetime metric tensor. We consider a non-magnetized pressureless plasma which is given by the plasma distribution (Bisnovatyi-Kogan & Tsupko (2010)) in which ω_p is the plasma electron frequency which equals, up to a scalar factor, the electron density,

$$\omega_p(x)^2 = \frac{4\pi e^2}{m_e} N_e(x), \tag{2}$$

where e and m_e are the electron charge and mass, respectively, and N_e is the electron number density. $x = (x^0, x^1, x^2, x^3)$ are the spacetime coordinates and $p = (p_0, p_1, p_2, p_3)$ are the canonical momentum coordinates. The light rays are the solutions to Hamilton's equations.

We then follow the formalism in which the photon momentum is decomposed into components parallel and orthogonal to the observer's four-velocity $U^\mu(x)$(Perlick & Tsupko (2017)), with the normalization condition $g_{\mu\nu}U^\mu U^\nu = -c^2$. Hence, the momentum can be written as

$$p^\mu = -\frac{1}{c}\,\omega(x)\,U^\mu(x) + k^\mu(x) \tag{3}$$

where $k^\mu(x)$ denotes the component orthogonal to the observer's four-velocity. This decomposition yields a covariant definition of the frequency,

$$\omega(x) = \frac{1}{c}\,p_\mu U^\mu(x), \tag{4}$$

and of the spatial wave vector,

$$k^\mu(x) = p^\mu + \frac{1}{c}\,\omega(x)\,U^\mu(x) \tag{5}$$

Using this orthogonal decomposition, the Hamiltonian constraint(substituting Eq. 3 in Eq. 1 and equating it to 0) leads to the dispersion relation(refer Perlick & Tsupko (2017)-Equations 5-8) for the details),

$$\omega(x)^2 = k_\mu(x)k^\mu(x) + \omega_p(x)^2, \tag{6}$$

since the wave vector defined in the Eq. 4, $k^\mu(x)$ is space-like and is positive in the (-,+,+,+) convention this further implies

$$\omega(x)^2 \geq \omega_p(x)^2, \tag{7}$$

where $\omega(x)$ is the photon frequency with respect to the plasma medium and ω_p is the plasma frequency i.e., light propagation is only possible for frequencies above the plasma frequency. We understand that the plasma is a dispersive medium, and light propagation depends on the plasma frequency.

2.2. *Solving in Kerr-Spacetime*

We will now specialize to the Kerr metric, which is given in Boyer–Lindquist coordinates $x = (t, r, \theta, \varphi)$, by

$$\begin{aligned} g_{\mu\nu}dx^\mu dx^\nu = &-c^2\left(1 - \frac{2mr}{\rho^2}\right)dt^2 + \frac{\rho^2}{\Delta}dr^2 + \rho^2 d\theta^2 \\ &+ \sin^2\theta\left(r^2 + a^2 + \frac{2mra^2\sin^2\theta}{\rho^2}\right)d\varphi^2 \\ &- \frac{4mra\sin^2\theta}{\rho^2}cdtd\varphi \end{aligned} \tag{8}$$

where

$$\Delta = r^2 + a^2 - 2mr, \qquad \rho^2 = r^2 + a^2\cos^2\theta \tag{9}$$

Here m is the mass parameter and a is the spin parameter,

$$m = \frac{GM}{c^2}, \qquad a = \frac{J}{Mc} \tag{10}$$

where M is the mass and J is the spin of the black hole. Throughout this paper, we assume that $a^2 \leq m^2$; i.e., we consider a black hole rather than a naked singularity. We restrict our consideration to the domain of outer communication, i.e., to the domain outside of the outer horizon,
$r > m + \sqrt{m^2 - a^2}$.

With the metric coefficients specified to the Kerr metric(refer Appendix 7.1 for the tensorial component of the Kerr Metric in the Boyer-Lindquist coordinates), the Hamiltonian (1) reads,

$$H = \frac{1}{2\rho^2}\left(\frac{1}{\Delta}\left(ap_\varphi + (r^2 + a^2)\frac{p_t}{c}\right)^2 \tag{11}$$

$$+ \left(\frac{p_\varphi}{\sin\theta} + a\sin^2\theta\frac{p_t}{c}\right)^2 + p_\theta^2 + \Delta p_r^2 + \rho^2\omega_p^2\Bigg) \tag{12}$$

In order to find the equation of motion for photons in the Kerr spacetime with a plasma, we must account for the plasma frequency. In the vacuum case $\omega_p(x) = 0$, there are four constants of the photon motion: the Hamiltonian $H = 0$, the total energy $E = -p_t$, the angular momentum $L = p_\varphi$, and the Carter constant given as

$$Q = p_\theta^2 - \cos^2\theta\left(a^2p_t^2 - \frac{p_\varphi^2}{\sin^2\theta}\right) \tag{13}$$

Provided these constants, the photon trajectories are uniquely determined, and one may obtain them by solving the Hamilton–Jacobi (H–J) equation.

However, this is no longer the case, in general, in the presence of plasma. For photons propagating in plasma, the Hamiltonian $H = 0$ still holds.

If we further assume that the plasma frequency ω_p is strictly only a function of r and θ, then from the Hamiltonian(1),

$$\frac{\partial H}{\partial t} = 0 \quad \text{and} \quad \frac{\partial H}{\partial \varphi} = 0, \text{ i.e., } p_t \text{ and } p_\varphi \text{ are constants of}$$

motion. Therefore, we obtain the constants of motion E=-p_t and L=p_ϕ same as above. Following the arguments in Perlick & Tsupko (2017), we also define w_0 to be the photon frequency measured at infinity, i.e., E=$\hbar\omega_0$. We use this for later reference to parametrize the dependence between the plasma and the light frequencies, respectively.

3. SEPARATION OF THE HAMILTON-JACOBI EQUATION

Similar to the case of a pure vacuum, the Hamilton–Jacobi formalism can be used to describe geodesic motion and to identify conserved quantities. In Kerr spacetime, separation of the Hamilton–Jacobi equation leads to the discovery of an additional constant of motion—the Carter constant—originally found by Brandon Carter, which arises from a hidden symmetry encoded in a Killing tensor(see Carter (1968)). Since much of what follows will be based on this result, we present Carter's argument, adapting it to Boyer-Lindquist coordinates.

So far, we have had three constants of motion. We now want to check the separability of the Hamilton-Jacobi equation in order to obtain the fourth constant (Carter constant). We substitute Eq. 12 in the Hamilton-Jacobi equation given by,

$$H\left(x, \frac{\partial S}{\partial x}\right) = 0 \tag{14}$$

by substituting Eq. 12 in Eq. 14, we get

$$\begin{aligned} 0 = & -\frac{1}{\Delta}\left(a\frac{\partial S}{\partial \varphi} + (r^2+a^2)\frac{1}{c}\frac{\partial S}{\partial t}\right)^2 \\ & + \left(\frac{1}{\sin\theta}\frac{\partial S}{\partial \varphi} + a\sin\theta\frac{1}{c}\frac{\partial S}{\partial t}\right)^2 \\ & + \left(\frac{\partial S}{\partial \theta}\right)^2 + \Delta\left(\frac{\partial S}{\partial r}\right)^2 + \rho^2\omega_p^2. \end{aligned} \tag{15}$$

Where we now use the separation ansatz given by,

$$S(t, \varphi, r, \theta) = \omega_0 t + p_\varphi \varphi + S_r(r) + S_\theta(\theta) \tag{16}$$

Here we work in natural units where $c = 1$ and $\hbar = 1$, so that all quantities are expressed in geometrized units. Upon substitution of this ansatz, the Hamilton–Jacobi equation takes the following form:

$$\begin{aligned} 0 = & -\frac{1}{\Delta}\Big(ap_\varphi + (r^2+a^2)\omega_0\Big)^2 + \Big(\frac{p_\varphi}{\sin\theta} + a\sin\theta\,\omega_0\Big)^2 \\ & + \big(S'_\theta(\theta)\big)^2 + \Delta\big(S'_r(r)\big)^2 + \omega_p^2(r^2 + a^2\cos^2\theta) \end{aligned} \tag{17}$$

It is clearly observed that the main criterion for the separability of the above equation is to write the expression in two terms, one only dependent on r while the other on θ. This enforces the condition on the plasma distribution for the separability of the Hamilton-Jacobi equation and hence, for the existence of the Carter constant being possible if and only if the plasma distribution is given as follows,

$$\omega_p(r, \vartheta)^2 = \frac{f_r(r) + f_\vartheta(\vartheta)}{r^2 + a^2\cos^2\vartheta} \tag{18}$$

where $f_r(r)$ is a function only dependent on r and $f_\vartheta(\vartheta)$ is a function only dependent on θ.

Now, the Hamiltonian can be separated into terms of only radial and angular dependence. In the Hamilton-Jacobi equation, for this equation to be equal to zero, both terms have to be constant, which is defined as the Carter constant(K) given by

$$\begin{aligned} K :=& \, p_\theta^2 + \big(a\omega_0\sin\theta - L\csc\theta\big)^2 + f_\theta(\theta) \\ =& \, -\Delta p_r^2 + \frac{1}{\Delta}\Big[(r^2+a^2)\omega_0 - aL\Big]^2 - f_r(r) \end{aligned} \tag{19}$$

Where we substituted for $S'_{x^i}(x^i) = p_{x^i}$, $E = -p_t$ and $L = p_\phi$. We have also used the term ω_0, which is defined as the photon frequency at infinity, and substituted for $E = \hbar\omega_0$, and conventionally put $\hbar = 1$.

We will now define following the general convention(Carter (1968)), the generalized Carter constant given as $Q = K - (L - aE)^2$ i.e.

$$Q = p_\theta^2 - \cos^2\theta\left(a^2\omega_0^2 - L^2\csc^2\theta\right) + f_\theta(\theta) \tag{20}$$

A similar expression for Q can also be obtained in terms of radial components using the same procedure. It is to be noticed in the Eq. 20 that, if $f_\theta(\theta)$ is a constant function, we have $Q - f_\theta(\theta) \geq 0$ for any photon passing through the equatorial plane since $Q - f_\theta(\theta) = p_\theta^2 \geq 0$ when $\theta = \pi/2$.

We conclude this section with one last expression, which is obtained from the Carter constant. Using Eq. 19, we can define functions

$$\mathcal{R}(r) = (r^2 + a^2 - a\xi)^2 - \Delta\big[\eta + (a-\xi)^2\big] - \Delta\,\hat{f}_r(r), \tag{21}$$

$$\Theta(\theta) = \eta + a^2\cos^2\theta - \xi^2\cot^2\theta - \hat{f}_\theta(\theta) \tag{22}$$

where $\mathcal{R}(r)$ and $\Theta(\theta)$ are the radial and angular potentials in a plasma medium. Note that in the limit where the plasma frequency approaches zero, we obtain the expressions for the radial and angular potentials in vacuum.

Refer to Appendix 7.3 for the derivation of these expressions, where we have used the following rescaled variables,

$$\xi = \frac{L}{\omega_0}, \quad \eta = \frac{Q}{\omega_0^2}, \quad \hat{f}_r = \frac{f_r}{\omega_0^2}, \quad \hat{f}_\theta = \frac{f_\theta}{\omega_0^2} \tag{23}$$

To summarise this section, the addition of a plasma term in the Hamiltonian of a photon makes the Hamilton-Jacobi equation non-separable in general. By assuming that the plasma obeys the condition given in Eq. 18, the equation of motion for photons can be obtained, and the influence of plasma appears only from the radial potential $\mathcal{R}(r)$ and angular potential $\Theta(\theta)$.

4. EXPRESSION FOR SHADOW ORBITS

In the previous sections, we have established the constants of motion, obtained expressions for the Carter constant, and then for the radial and angular potentials. Now we use these expressions to confine the photon region and then finally obtain the expressions for the shadows using celestial coordinates (also known as impact parameters in the literature) Bardeen (1973) (refer to Appendix 7.2 for a quick review).

Now, to begin with the derivation, note that the boundary of a black hole's shadow is determined by the fate of photons on unstable spherical orbits. These are null geodesics that remain at a constant coordinate radius, r, forming a photon shell (or photon region) around the black hole. The orbits are unstable because they represent a critical balance: a slight perturbation inward will cause the photon to spiral across the event horizon, while a slight perturbation outward will allow it to escape to infinity. Consequently, a distant observer sees this separatrix between captured and escaping orbits as the sharp edge of the shadow.

This implies that the spherical light rays satisfy the condition,

$$\mathcal{R}(r) = \mathcal{R}'(r) = 0 \tag{24}$$

where the prime denotes derivative. Solving these two equations, we have (refer to Appendix 7.4 for details)

$$\xi = -\frac{M(a^2 - r^2) + \Delta r\sqrt{1-\delta}}{a(r-M)} \tag{25a}$$

$$\eta = \frac{r^3}{a^2(r-M)^2}\Bigg\{ 2M\Delta(1+\sqrt{1-\delta}) - r(r-M)^2 + (r-2M)\Delta\delta - \frac{a^2(r-M)^2}{r^3}\hat{f}_r(r)\Bigg\} \tag{25b}$$

where we have introduced

$$\delta = \frac{r-M}{2r^2}\hat{f}_r(r) \tag{26}$$

As discussed below Eq. 20, a photon orbit crossing the equatorial plane should satisfy

$$\eta - \hat{f}_\theta(\theta) \geq 0 \tag{27}$$

Above equation helps us to confine all the photon orbits that cross the equatorial plane(θ=$\pi/2$). By substituting Eq .(24b) in Eq. 27, we obtain the expression for the photon orbits(only those that can cross the equatorial plane due to the constraint Eq. 27).

We will now introduce the impact parameters (α and β) mentioned at the beginning of the section to describe the image of the shadow on the observer's sky. Following the details in the Appendix 7.5, we obtain the following expressions.

$$\alpha(r) = -\frac{\xi(r)}{\sin\theta_o} \tag{28a}$$

$$\beta(r) = \pm\sqrt{\eta(r) + a^2\cos^2\theta_o - \xi(r)^2\cot^2\theta_o - \hat{f}_\theta(\theta_o)} = \pm\sqrt{\Theta(\theta_o)} \tag{28b}$$

where the parameter r ranges over the photon sphere described above and θ_0 is the angle of the observer with respect to the black hole in Boyer–Lindquist coordinates(Bardeen (1973)). Now from Eqn (27a) and (27b), we substitute Eqn (24a) and (24b) to obtain the following,

$$\alpha(r) = \frac{M(a^2 - r^2) + \Delta r\sqrt{1-\delta}}{a(r-M)}\csc\theta_0 \tag{29a}$$

$$\beta(r) = \pm\Bigg[\frac{r^3}{a^2(r-M)^2}\Bigg\{2M\Delta\Big(1+\sqrt{1-\delta}\Big) - r(r-M)^2 + (r-2M)\Delta\,\delta - \frac{a^2(r-M)^2}{r^3}\hat{f}_r(r)\Bigg\} + a^2\cos^2\theta_0 - \xi(r)^2\cot^2\theta_0 - \hat{f}_\theta(\theta_0)\Bigg]^{1/2} \tag{29b}$$

These are the final equations that we require to get the shadow of a black hole on the observer's sky, which are described in the (α,β) coordinate axes.

5. PLASMA MODELS AND COMPUTATION OF SHADOWS

We have now derived all the equations that are necessary for the calculation of the shadow boundary of a Kerr black hole in a plasma medium with the constraint given in Eq. 18.

Our investigation now turns to the application of these equations, where we characterize the shadow for various plasma models that adhere to the separability condition Eq. 18.

We start with the following models for the plasma density, In model 1, we have plasma density with $f_r(r) = \omega^2M^2$, $f_\theta(\theta) = 0$ such that $\omega_p^2 \sim \frac{1}{r^2}$ at large r,

$$\omega_p(r,\theta)^2 = \frac{\omega_c^2M^2}{r^2 + a^2\sin^2\theta}. \tag{30}$$

In model 2, we have plasma density with $f_r(r) = \omega_c^2Mr$, $f_\theta(\theta) = 0$ such that $\omega_p^2 \sim \frac{1}{r}$ at large r,

$$\omega_p(r,\theta)^2 = \frac{\omega_c^2Mr}{r^2 + a^2\sin^2\theta}. \tag{31}$$

In model 3, we have the plasma density with $f_r(r) = \omega_c^2(M^3r)^{1/2}$, $f_\theta(\theta) = 0$

$$\omega_p(r,\theta)^2 = \frac{\omega_c^2(M^3r)^{1/2}}{r^2 + a^2\sin^2\theta}. \tag{32}$$

In model 4, we have the plasma density with $f_r(r) = \omega^2Mr^2$, $f_\theta(\theta) = 0$

$$\omega_p(r,\theta)^2 = \frac{\omega_c^2Mr^2}{r^2 + a^2\sin^2\theta}. \tag{33}$$

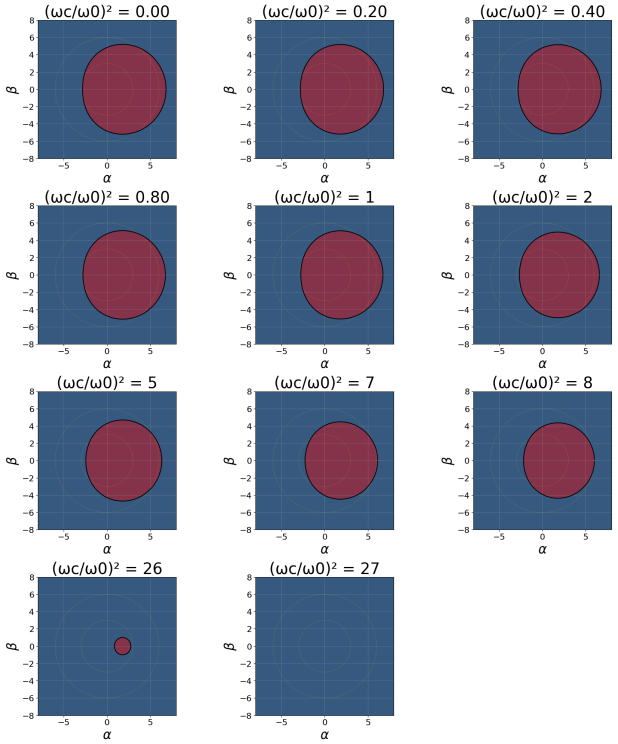

Figure 1. Shadow boundaries of a black hole in the model$f_r(r) = \omega^2 M^2, f_\theta(\theta) = 0$. The black hole spin is a/m = 0.9 and observer inclination is $\theta_0 = 90°$. The red region marks the shadow interior. For low plasma effects, the shadow resembles the vacuum case, but it gradually shrinks as $(\omega_p/\omega)^2$ increases. Once the critical value $(\omega_p/\omega)^2 \approx 26$ is reached, corresponding to photon frequencies below the critical frequency ω_c, the shadow disappears completely.

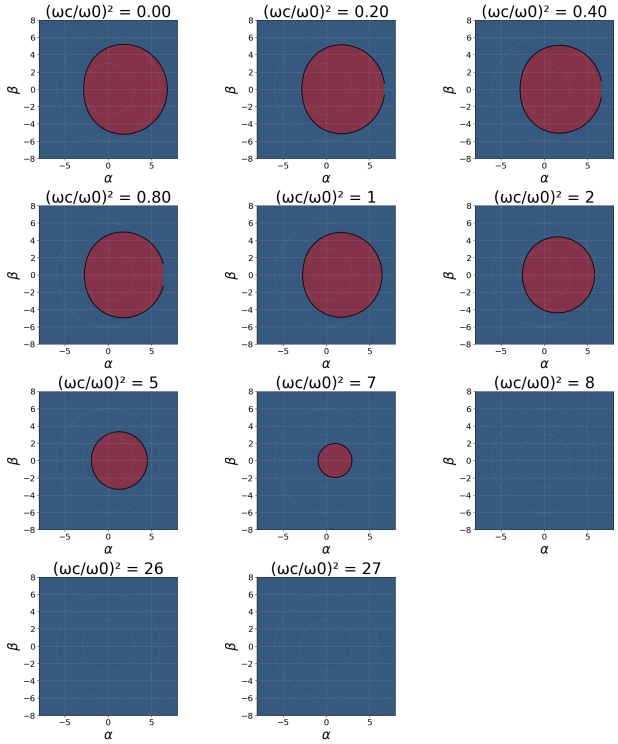

Figure 2. Shadow boundaries of a black hole in the model $f_r(r) = \omega^2 Mr$, $f_\theta(\theta) = 0$. The color scheme is the same as in Fig. 1. The black hole spin is a/m = 0.9 and observer inclination is $\theta_0 = 90°$. Once the critical value $(\omega_p/\omega)^2 \approx 8$ is reached, corresponding to photon frequencies below the critical frequency ω_c, the shadow disappears completely

Following a similar convention as given in Yan (2019), we have used a constant ω_c in these models. For later reference, we also used a rescaled constant, $\hat{\omega}_c = \omega_c/\omega_0$.

We name the plasma distributions with the form of Eq. 30, Eq. 31, Eq. 32 and Eq. 33 as the power-law-like models for the reason that the distributions are approximately the same as the power-law models at large r (asymptotically large distance).

Since we are interested in the optical appearance of a black hole, we may expect the existence of a light ray anywhere outside of the black hole. Light propagation in a plasma does depend on the photon frequency ω_0 (see the discussion following Eqn (10) in Yan (2019)). The condition from Eq. 7 gives a constraint between the plasma frequency ω_p and the photon frequency ω_0. It is to be highly emphasized that the relevant quantity to describe a photon trajectory (and thus the observables) is the ratio of plasma frequency and photon frequency, which can be represented by the term $\hat{\omega}_c$ for the above models (for more elaborate discussion, refer to Yan (2019) section II, B.Plasma models). We can interpret these in either of the following ways: if we consider only the photons with a given frequency, different ratios represent different case studies of plasmas with different densities. On the other hand, for a given plasma distribution, different ratios represent the chromatic effect of the plasma. For all the above models, we always have $\omega_p < \omega_c$. Therefore, the photon trajectory is similar, as it would propagate in vacuum spacetime if $\hat{\omega}_c \ll 1$. However, if $\hat{\omega}_c \gg 1$, it is even impossible for a photon to propagate in the plasma (this is just a restatement of Eq. 7). Even though the plasma models discussed here are highly idealized, it is possible to extract some approximate effects of a real plasma by using these toy models.

6. CONCLUSION

In this paper, we have investigated the propagation of light rays in non-magnetized, pressureless cold plasma in Kerr Spacetime. We have worked within the frame-

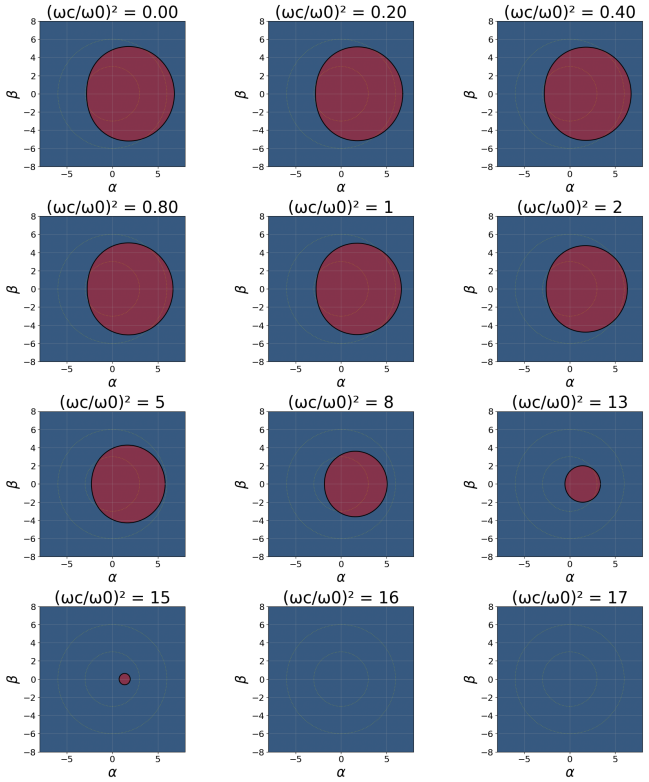

Figure 3. Shadow boundaries of a black hole in the model $f_r(r) = \omega_c^2(M^3r)^{1/2}$, $f_\theta(\theta) = 0$. The color scheme is the same as in Fig. 1.The black hole spin is a/m = 0.9 and observer inclination is $\theta_0 = 90°$. Once the critical value $(\omega_p/\omega)^2 \approx 16$ is reached, corresponding to photon frequencies below the critical frequency ω_c, the shadow disappears completely.

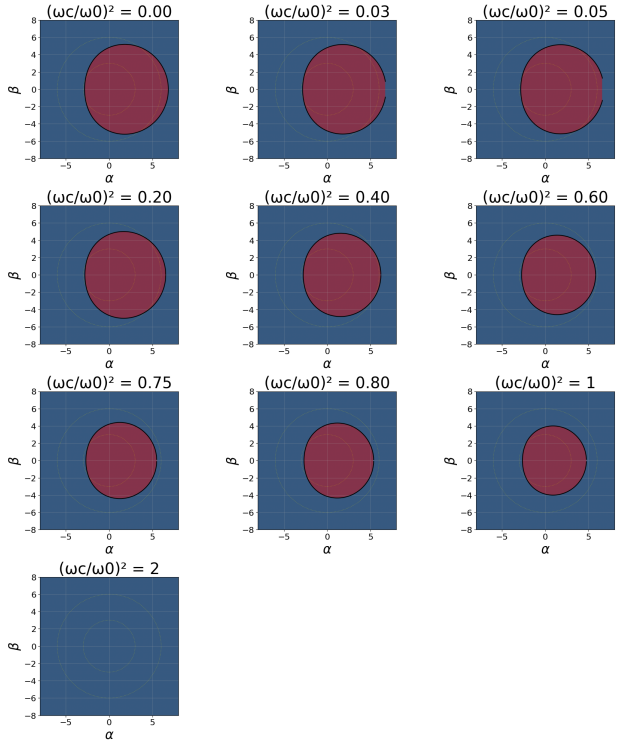

Figure 4. Shadow boundaries of a black hole in the model $f_r(r) = \omega^2 Mr^2$. The color scheme is the same as in Fig. 1. The black hole spin is a/m = 0.9 and observer inclination is $\theta_0 = 90°$. Once the critical value $(\omega_p/\omega)^2 \gtrsim 1$ is reached, corresponding to photon frequencies below the critical frequency ω_c, the shadow disappears completely.

work of geometrical optics, considering the plasma as a dispersive medium with properties that are frequency-dependent. The gravitational field is determined by the mass and the spin of the Kerr black hole; i.e., the gravitational field of the plasma particles is not taken into account. In this paper, the presence of the plasma manifests itself only in a change of the trajectories of light rays. This is valid for any value of the spin parameter a and for any light rays that cross the equatorial plane of the black hole (θ=$\pi/2$) and observed by an observer at infinity (impact parameters or screen coordinates). As the plasma is a dispersive medium, photons with different frequencies move along different trajectories. We have demonstrated the frequency dependence of light for various models under consideration.

We have utilised the Hamiltonian formalism for light rays in a plasma on Kerr spacetime, and we have, in an important first step of our analysis, determined the necessary and sufficient condition for separability of the Hamilton-Jacobi equation; see Sections 2 and 3. We have demonstrated that the Hamilton-Jacobi equation is separable, i.e., that a generalised Carter constant exists, only for special distributions of the plasma electron density. The sufficient condition for separability is given in Eq. 18, which we used for different models.

We then derived the equations of motion using the Hamilton-Jacobi condition for light propagation, as well as the equations of spherical light rays corresponding to the photon sphere; see Sec 4. We have derived the analytical formulas for the boundary curve of the shadow in the observer's sky in terms of the impact parameters, see Eq. (28a) and (28b). Most derivations for the equations are provided in the Appendix for convenience. We have then shown the plots for the shadows formed for different models of plasma distributions in the Kerr space-time and have evaluated the critical frequency($\hat{\omega}_c$) above which the light rays no longer propagate; see Section 5.

In this paper, the plasma influences only the trajectories of light rays, which results in changes to the geometrical size and shape of the shadow. We have not

taken into account processes of absorption or scattering of photons, nor have we considered more complex plasma effects such as magnetization or thermal distributions, which would require numerical ray-tracing methods beyond our geometrical optics approach.

Our goal here was to derive analytical formulas for the shadow boundary under idealized conditions, specifically for observers at infinity. For a more general treatment using tetrad formalism that applies to observers at finite distances from the black hole, see Perlick & Tsupko (2017). It is verified through this work that in the presence of a plasma around a black hole, the size and the shape of the shadow differ from the vacuum case in a way that depends on the photon frequency. The relevant quantity is the ratio of the plasma frequency to the photon frequency. From our examples, we conclude that if the plasma frequency is small compared to the photon frequency, the shadow is not significantly different from the vacuum case. However, if the plasma frequency is close to the photon frequency, the properties of the shadow are changed drastically because of significant changes in the photon regions.

The analytical approach developed in this work provides a framework for systematically studying the effects of plasma on black hole shadows. While numerical ray-tracing methods offer greater flexibility for arbitrary plasma distributions, our approach yields closed-form expressions that clearly reveal the dependence on physical parameters. This enables efficient parameter studies and offers physical insight that might be obscured in purely numerical treatments. The separability condition we derived serves as a benchmark against which more complex scenarios can be compared, and our results establish baseline expectations for future observational campaigns aimed at detecting plasma effects in black hole shadows.

This analytical framework was developed to complement the growing body of numerical ray-tracing studies of black hole shadows in plasma environments. While numerical approaches (e.g., Mizuno 2018) offer greater flexibility for arbitrary plasma distributions, they often require substantial computational resources and can obscure the fundamental parameter dependencies that analytical solutions reveal. Our approach provides a mathematical foundation for understanding how plasma affects black hole shadows, establishing the separability condition (Eq. 18) as a theoretical benchmark. The closed-form expressions we derive for shadow boundaries (Eq. 28a and 29b) enable rapid parameter studies and facilitate direct comparison with analytical results in the vacuum limit. Future work could extend this approach to include more complex plasma effects while maintaining some degree of analytical tractability through perturbative methods around our separable solutions.

Looking forward, this work provides a foundation for several important extensions. The most immediate is to move beyond the separability condition by developing numerical ray-tracing techniques for arbitrary plasma distributions from GRMHD simulations, which would allow us to quantify degeneracies with black hole parameters like spin and inclination. Furthermore, modelling dynamic plasma environments with stochastic or periodic variations would capture the turbulent nature of real accretion flows. An observationally critical next step is to investigate the chromaticity of the shadow across the mm-wave band to produce testable predictions for next-generation instruments like the ngEHT. Finally, coupling this ray-tracing with radiative transfer calculations to generate synthetic intensity and polarization maps will be essential for direct comparison with interferometric data from the EHT and other VLBI arrays.

ACKNOWLEDGEMENTS

SKM and SKK thank the support from the INSPIRE faculty grant from the Department of Science and Technology, India (DST/INSPIRE/04/2023/000401)
SKM also extends heartfelt thanks to the SPASE Department at IIT Kanpur for their unwavering support and for providing an enriching academic environment that made this study possible.

REFERENCES

Abdujabbarov, A., Amir, M., Ahmedov, B., & Ghosh, S. G. 2016, Phys. Rev. D, 93, 104004, doi: 10.1103/PhysRevD.93.104004

Amarilla, L., & Eiroa, E. F. 2010, Phys. Rev. D, 81, 124045, doi: 10.1103/PhysRevD.81.124045

Amarilla, L., Eiroa, E. F., & Giribet, G. 2010, Phys. Rev. D, 81, 124045, doi: 10.1103/PhysRevD.81.124045

Bardeen, J. M. 1973, in Black Holes (Les Houches 1972), ed. C. DeWitt & B. S. DeWitt (New York: Gordon and Breach), 215–239

Bisnovatyi-Kogan, G. S., & Tsupko, O. Y. 2010, Monthly Notices of the Royal Astronomical Society, 404, 1790, doi: 10.1111/j.1365-2966.2010.16290.x

Carter, B. 1968, Physical Review, 174, 1559, doi: 10.1103/PhysRev.174.1559

Cunha, P. V. P., & Herdeiro, C. A. R. 2018, Gen. Rel. Grav., 50, 42, doi: 10.1007/s10714-018-2361-9

Cunha, P. V. P., Herdeiro, C. A. R., & Radu, E. 2017a, Phys. Rev. D, 96, 024039, doi: 10.1103/PhysRevD.96.024039

—. 2017b, Phys. Rev. D, 96, 024039, doi: 10.1103/PhysRevD.96.024039

Event Horizon Telescope Collaboration. 2019, Astrophysical Journal Letters, 875, L1, doi: 10.3847/2041-8213/ab0ec7

—. 2022, Astrophysical Journal Letters, 930, L12, doi: 10.3847/2041-8213/ac6674

Hioki, K., & Maeda, K.-i. 2009, Phys. Rev. D, 80, 024042, doi: 10.1103/PhysRevD.80.024042

Johannsen, T. 2016, Class. Quantum Grav., 33, 124001, doi: 10.1088/0264-9381/33/12/124001

Johannsen, T., & Psaltis, D. 2010, Astrophys. J., 718, 446, doi: 10.1088/0004-637X/718/1/446

Kerr, R. P. 1963, Physical Review Letters, 11, 237, doi: 10.1103/PhysRevLett.11.237

Luminet, J. P. 1979, A&A, 75, 228

Mizuno, Y. e. a. 2018, Nat. Astron., 2, 585, doi: 10.1038/s41550-018-0449-5

Perlick, V., & Tsupko, O. Y. 2015, Phys. Rev. D, 92, 104031, doi: 10.1103/PhysRevD.92.104031

—. 2017, Physical Review D, 95, doi: 10.1103/physrevd.95.104003

Schwarzschild, K. 1916, Sitzungsber. Preuss. Akad. Wiss. Berlin (Math. Phys.), 1916, 189. https://arxiv.org/abs/physics/9905030

Synge, J. L. 1966, Monthly Notices of the Royal Astronomical Society, 131, 463, doi: 10.1093/mnras/131.3.463

Tsukamoto, N., Li, Z., & Bambi, C. 2014, JCAP, 2014, 043, doi: 10.1088/1475-7516/2014/06/043

Yan, H. 2019, Phys. Rev. D, 99, 084050, doi: 10.1103/PhysRevD.99.084050

7. APPENDIX

7.1. *Kerr Metric Tensor*

The Kerr metric describes the geometry of spacetime around a rotating black hole of mass M and angular momentum per unit mass a. In Boyer–Lindquist coordinates (t, r, θ, ϕ), the line element is

$$\begin{aligned} ds^2 = &-\left(1 - \frac{2Mr}{\Sigma}\right) dt^2 - \frac{4Mar\sin^2\theta}{\Sigma}\, dt\, d\phi + \frac{\Sigma}{\Delta} dr^2 + \Sigma\, d\theta^2 \\ &+ \left(r^2 + a^2 + \frac{2Ma^2 r \sin^2\theta}{\Sigma}\right) \sin^2\theta\, d\phi^2 \end{aligned} \tag{A1}$$

where the metric functions are defined as

$$\Delta = r^2 - 2Mr + a^2 \tag{A2}$$

$$\Sigma = r^2 + a^2\cos^2\theta \tag{A3}$$

The non-vanishing covariant components of the Kerr metric tensor $g_{\mu\nu}$ are therefore

$$g_{tt} = -\left(1 - \frac{2Mr}{\Sigma}\right) \tag{A4a}$$

$$g_{t\phi} = -\frac{2Mar\sin^2\theta}{\Sigma} \tag{A4b}$$

$$g_{rr} = \frac{\Sigma}{\Delta} \tag{A4c}$$

$$g_{\theta\theta} = \Sigma \tag{A4d}$$

$$g_{\phi\phi} = \left(r^2 + a^2 + \frac{2Ma^2 r\sin^2\theta}{\Sigma}\right)\sin^2\theta \tag{A4e}$$

7.2. *Screen coordinates*

The screen coordinates (α, β) on the celestial sphere can be derived from the photon's constants of motion. Following the approach in Yan (2019), we begin with the tetrad formalism for an observer at position (r_o, θ_o).

The appropriate ZAMO (Zero Angular Momentum Observer) tetrad for Kerr spacetime is given by:

$$e_{(0)} = \sqrt{\frac{\Sigma}{\Delta}} \left(\frac{\partial_t + \frac{2aMr}{\Sigma^2}\partial_\phi}{\sqrt{1 - \frac{2Mr}{\Sigma}}} \right) \tag{34}$$

$$e_{(1)} = \sqrt{\frac{\Delta}{\Sigma}}\partial_r \tag{35}$$

$$e_{(2)} = \frac{1}{\sqrt{\Sigma}}\partial_\theta \tag{36}$$

$$e_{(3)} = \frac{\sin\theta}{\sqrt{\Sigma}}\partial_\phi \tag{37}$$

This tetrad represents the observer's local reference frame, with $e_{(0)}$ aligned with their four-velocity and $e_{(1)}$, $e_{(2)}$, $e_{(3)}$ forming an orthonormal spatial basis. For detailed discussion of tetrad construction in Kerr spacetime, see Bardeen (1973).

The photon's four-momentum components in this frame are:

$$p^{(0)} = -e^{\mu}_{(0)} p_{\mu} \tag{38}$$
$$p^{(1)} = e^{\mu}_{(1)} p_{\mu} \tag{39}$$
$$p^{(2)} = e^{\mu}_{(2)} p_{\mu} \tag{40}$$
$$p^{(3)} = e^{\mu}_{(3)} p_{\mu} \tag{41}$$

The screen coordinates are then defined as the apparent angular displacements on the celestial sphere:

$$\alpha = -\lim_{r_o \to \infty} \left(r_o \frac{p^{(3)}}{p^{(1)}} \right) \tag{42}$$
$$\beta = \lim_{r_o \to \infty} \left(r_o \frac{p^{(2)}}{p^{(1)}} \right) \tag{43}$$

Substituting the conserved quantities $\xi = L/\omega_0$ and $\eta = Q/\omega_0^2$, and taking the limit $r_o \to \infty$, we obtain the final expressions:

$$\alpha = -\frac{\xi}{\sin\theta_o} \tag{B1}$$
$$\beta = \pm\sqrt{\eta + a^2\cos^2\theta_o - \xi^2\cot^2\theta_o - \hat{f}_\theta(\theta_o)} \tag{B2}$$

These coordinates describe the apparent position on the observer's sky, with α perpendicular to the spin axis and β parallel to it. The inclusion of $\hat{f}_\theta(\theta_o)$ accounts for the plasma's influence on the photon's apparent position.

7.3. *Derivation of the Radial and Angular Potentials*

Starting from the definition of the Carter constant in Eq. (18):

$$K = p_\theta^2 + (a\omega_0 \sin\theta - L\csc\theta)^2 + f_\theta(\theta) = -\Delta p_r^2 + \frac{1}{\Delta}\left[(r^2+a^2)\omega_0 - aL\right]^2 - f_r(r) \tag{44}$$

we introduce the rescaled variables from Eq. (23):

$$\xi = \frac{L}{\omega_0}, \quad \eta = \frac{K - (L - a\omega_0)^2}{\omega_0^2}, \quad \hat{f}r = \frac{f_r}{\omega_0^2}, \quad \hat{f}\theta = \frac{f_\theta}{\omega_0^2} \tag{45}$$

7.3.1. *Radial Potential $\mathcal{R}(r)$*

Beginning with the radial part:

$$\eta + (\xi - a)^2 = -\Delta p_r^2 + \frac{1}{\Delta}\left[(r^2+a^2) - a\xi\right]^2 - \hat{f}_r(r) \tag{46}$$

Rearranging terms:

$$\Delta p_r^2 = \frac{1}{\Delta}\left[(r^2+a^2) - a\xi\right]^2 - \left[\eta + (\xi - a)^2 + \hat{f}_r(r)\right] \tag{47}$$

Multiplying through by Δ:

$$\Delta^2 p_r^2 = \left[(r^2+a^2) - a\xi\right]^2 - \Delta\left[\eta + (\xi - a)^2 + \hat{f}_r(r)\right] \tag{48}$$

We thus define the radial potential as:

$$\mathcal{R}(r) = \left[(r^2+a^2) - a\xi\right]^2 - \Delta\left[\eta + (\xi - a)^2 + \hat{f}_r(r)\right] \tag{49}$$

which matches Eq. (21) in the main text.

7.3.2. *Angular Potential* $\Theta(\theta)$

Now considering the angular part:

$$\eta + (\xi - a)^2 = p_\theta^2 + (a\sin\theta - \xi\csc\theta)^2 + \hat{f}_\theta(\theta) \tag{50}$$

Expanding the squared term:

$$(a\sin\theta - \xi\csc\theta)^2 = a^2\sin^2\theta - 2a\xi + \xi^2\csc^2\theta \tag{51}$$

Substituting back:

$$\eta + (\xi - a)^2 = p_\theta^2 + a^2\sin^2\theta - 2a\xi + \xi^2\csc^2\theta + \hat{f}_\theta(\theta) \tag{52}$$

Note that $(\xi - a)^2 = \xi^2 - 2a\xi + a^2$, so:

$$\eta + \xi^2 - 2a\xi + a^2 = p_\theta^2 + a^2\sin^2\theta - 2a\xi + \xi^2\csc^2\theta + \hat{f}_\theta(\theta) \tag{53}$$

Cancelling $-2a\xi$ on both sides:

$$\eta + \xi^2 + a^2 = p_\theta^2 + a^2\sin^2\theta + \xi^2\csc^2\theta + \hat{f}_\theta(\theta) \tag{54}$$

Rewriting and using the identity $a^2 - a^2\sin^2\theta = a^2\cos^2\theta$:

$$p_\theta^2 = \eta + a^2\cos^2\theta - \xi^2\cot^2\theta - \hat{f}_\theta(\theta) \tag{55}$$

We thus define the angular potential as:

$$\Theta(\theta) = \eta + a^2\cos^2\theta - \xi^2\cot^2\theta - \hat{f}_\theta(\theta), \tag{56}$$

which matches Eq. (21) in the main text.

7.4. *Derivation of Spherical Photon Orbit Parameters*

For spherical photon orbits, we require:

$$\mathcal{R}(r) = 0 \quad \text{and} \quad \frac{d\mathcal{R}}{dr} = 0 \tag{57}$$

From Eq. (20), the radial potential is:

$$\mathcal{R}(r) = \left[(r^2 + a^2) - a\xi\right]^2 - \Delta\left[\eta + (a - \xi)^2 + \hat{f}_r(r)\right] = 0. \tag{A1}$$

Differentiating $\mathcal{R}(r)$ with respect to r:

$$\begin{aligned}\frac{d\mathcal{R}}{dr} =& 2\left[(r^2 + a^2) - a\xi\right](2r) - \frac{d\Delta}{dr}\left[\eta + (a - \xi)^2 + \hat{f}_r(r)\right] \\ & - \Delta\frac{d}{dr}\left[\eta + (a - \xi)^2 + \hat{f}_r(r)\right] = 0,\end{aligned} \tag{A2}$$

where $\frac{d\Delta}{dr} = 2(r - M)$.

To solve equations (A1) and (A2), we follow the approach in Perlick & Tsupko (2015) and introduce the function:

$$\delta(r) = \frac{r - M}{2r^2}\hat{f}_r(r), \tag{58}$$

which corresponds to Eq. (26) in the main text.

Using this definition, the solutions for the impact parameters that satisfy both R(r) = 0 and R'(r) = 0 are found to be the solutions for the impact parameters and are given as:

$$\xi = -\frac{M(a^2 - r^2) + \Delta r\sqrt{1 - \delta}}{a(r - M)}, \tag{A3}$$

$$\eta = \frac{r^3}{a^2(r - M)^2}\left[2M\Delta(1 + \sqrt{1 - \delta}) - r(r - M)^2 + (r - 2M)\Delta\delta - \frac{a^2(r - M)^2}{r^3}\hat{f}_r(r)\right] \tag{A4}$$

These expressions match Eqs. (24a) and (24b) in the main text and describe the parameters for spherical photon orbits in the presence of a plasma distribution satisfying the separability condition.

7.5. *Screen Coordinates for Observers at Infinity*

For an observer at infinity ($r_o \to \infty$), the screen coordinates (α, β) can be derived from the tetrad formalism in Bardeen (1973). The general expressions are:

$$\alpha = -\frac{\xi}{\sin\theta_o}, \tag{A5}$$

$$\beta = \pm\sqrt{\eta + a^2\cos^2\theta_o - \xi^2\cot^2\theta_o - \hat{f}_\theta(\theta_o)} \tag{A6}$$

Substituting the expressions for ξ and η from Eqs. (A3) and (A4) into these definitions yields the explicit forms:

$$\alpha(r) = \frac{M(a^2 - r^2) + \Delta r\sqrt{1-\delta}}{a(r-M)}\csc\theta_0, \tag{A7}$$

$$\beta(r) = \pm\left[\frac{r^3}{a^2(r-M)^2}\left(2M\Delta(1+\sqrt{1-\delta}) - r(r-M)^2 + (r-2M)\Delta\delta - \frac{a^2(r-M)^2}{r^3}\hat{f}r(r)\right) + a^2\cos^2\theta_0 - \xi(r)^2\cot^2\theta_0 - \hat{f}\theta(\theta_0)\right] \tag{A8}$$

These equations correspond to Eqs. (28a) and (28b) in the main text and provide the complete description of the shadow boundary in the observer's sky for Kerr black holes surrounded by separable plasma distributions.